Advances in Applied Mathematics and Mechanics
Adv. Appl. Math. Mech., Vol. **9**, No. 3, pp. 621-650

DOI: 10.4208/aamm.2015.m1340
June 2017

1D Exact Elastic-Perfectly Plastic Solid Riemann Solver and Its Multi-Material Application

Si Gao and Tiegang Liu*

LMIB and School of Mathematics and Systems Science, Beihang University, Beijing 100191, China

Received 11 November 2015; Accepted (in revised version) 14 June 2016

Abstract. The equation of state (EOS) plays a crucial role in hyperbolic conservation laws for the compressible fluid. Whereas, the solid constitutive model with elastic-plastic phase transition makes the analysis of the solid Riemann problem more difficult. In this paper, one-dimensional elastic-perfectly plastic solid Riemann problem is investigated and its exact Riemann solver is proposed. Different from previous works treating the elastic and plastic phases integrally, we resolve the elastic wave and plastic wave separately to understand the complicate nonlinear waves within the solid and then assemble them together to construct the exact Riemann solver for the elastic-perfectly plastic solid. After that, the exact solid Riemann solver is associated with the fluid Riemann solver to decouple the fluid-solid multi-material interaction. Numerical tests, including gas-solid, water-solid high-speed impact problems are simulated by utilizing the modified ghost fluid method (MGFM).

AMS subject classifications: 35L50, 35Q74, 74C05, 74F10, 74M20

Key words: Riemann problem, elastic-plastic solid, ghost fluid method, multi-material flows.

1 Introduction

In recent decades, exact and approximate Riemann solvers have been carefully designed to calculate the Riemann problem and provide the numerical fluxes across the interfaces of computing cells. Godunov firstly introduced a conservative method which defined the numerical fluxes by solving local Riemann problems to settle the non-linear systems of conservation laws [1]. In the original Godunov method, local Riemann problems are solved accurately. As the iterative procedure of the exact Riemann solver is rather time-consuming, alternatively, approximate and non-iterative Riemann solvers are developed to evaluate the numerical fluxes approximately. On one hand, approximate

*Corresponding author.
Email: gaos@buaa.edu.cn (S. Gao), liutg@buaa.edu.cn (T. G. Liu)

 ©2017 Global Science Press

https://doi.org/10.4208/aamm.2015.m1340 Published online by Cambridge University Press

state-based Riemann solvers such as double-shock Riemann solver, double-rarefaction Riemann solver, and their hybrid versions [2] are employed to define the fluxes indirectly. On the other hand, approximate flux-based Riemann solvers, for instance, HLL-type Riemann solvers [3–6], Roe Riemann solver [7] and Osher Riemann solver [8, 9], estimate the fluxes directly. These two classes of approximate Riemann solvers have been widely adopted in hydrodynamics codes nowadays.

However, in this work, we study the exact Riemann solvers for the elastic-perfectly plastic solid and its multi-material interfaces. The reason is twofold. Firstly, as complex nonlinear waves arise in the elastic-plastic solid, the intensive study of the exact solution can provide a more reliable result and an initial foothold for the further more efficient approximate solution theoretically. Secondly, the exact Riemann solver is intended to treat the multi-material interaction by the MGFM approach [10–12] instead of developing a Godunov-type scheme. Since MGFM is a multi-material method which needs to solve only one local Riemann problem at the multi-material interface during each time step, the time-consuming effect is limited.

Actually, for purpose of solving the solid Riemann problem, a number of exact or approximate Riemann solvers based on the specific solid assumptions have been proposed. Regarding to the elastic solid, Kaboudian and Khoo [13] analysed the elastic solid Riemann problem in the Lagrangian framework and put forward a Riemann solver according to the characteristic theory. As for the nonlinear elasticity, multiple approaches have been implemented. LeFloch [14] only utilized shock waves to approximate the original Riemann problem structure. Garaizar [15] demonstrated an exact Riemann problem solution of isotropic hyperelastic material theoretically without performance demonstration by numerical results. Miller [16] presented a general iterative Riemann solver and applied it to the hyperelastic material. The great discrepancy between the exact and approximate solutions indicates that the exact solution is a necessity for the complex solid flow. Barton et al. [17] achieved high-order spatial accuracy by the monotonicity preserving weighted essentially non-oscillatory (MPWENO) reconstruction and the local Riemann problem characteristic decomposition. HLLD Riemann solver was implemented by López Ortega et al. [18] and then was extended to the multi-material circumstance. Considering the elastic-plastic solid, Trangenstein and Pember [19] illustrated an analytical solution to the Riemann problem for Antman-Szymczak model which described the elastic-plastic material. Lin [20] raised an iterative procedure to calculate the Riemann problem approximately by linearizing the Riemann invariants. Whereas Wang et al. [21] adopted the fully conservative Eulerian formulation for elasto-plasticity proposed in [22] and employed an approximate Riemann solver via right eigenvectors decomposition based on constant coefficient systems. Miller and Colella [23] also took the similar approach to construct a high-order Godunov method for the elastic-plastic flow in solid solved in nonconservative form depending on the work of Trangenstein and Colella [24].

A large part of the methods illustrated above introduce the deformation tensor and formulate a hyperbolic conservative system with variables like inverse deformation gradient, mass, momentum, energy, even work-hardening, plastic strain tensor, etc. Consid-

https://doi.org/10.4208/aamm.2015.m1340 Published online by Cambridge University Press

ering the traditional elastic-perfectly plastic solid model surveyed by Wilkins [25], since the elastic to plastic phase transition blends into the conservation laws, the analytical solution of this system is extraordinary intricate. In this paper, we switch the thought pattern and investigate the elastic wave and plastic wave respectively to avoid the nonuniformity in the constitutive models. Besides, the constitutive models are transformed into the Eulerian form and then an integrated non-conservative hyperbolic system is formulated, consisting primitive variables like density, velocity, hydrostatic pressure and deviatoric stress, which can facilitate the deduction of mathematical properties and the final exact elastic-perfectly plastic solid Riemann solver.

This paper is organized as follows. In Section 2, we discuss the exact Riemann solver for the elastic solid. Parallelly, the exact Riemann solver for the perfectly plastic material is presented in Section 3. In Section 4, the shock and rarefaction relationships for the elastic wave and plastic wave are assembled as the final Riemann solver for the elastic-perfectly plastic solid. In Section 5, we verify the accuracy of the above exact Riemann solvers. In Section 6, the multi-material extension is discussed and its numerical results are demonstrated in Section 7. Finally, conclusions are summarized in Section 8.

2 The elastic waves and the exact elastic solid-solid Riemann solver

In this section, we put forward the elastic wave relationship and obtain the exact elastic solid-solid Riemann solver which will be provided as a foundation to construct the elastic-perfectly plastic solid-solid Riemann solver proposed in Section 4.

2.1 Governing equations and constitutive models for the elastic solid

The one-dimensional nonlinear system of hyperbolic conservation laws with source terms, neglecting the effects of body forces, viscous stresses and heat-conducting, to describe the elastic solid in the Eulerian coordinate system is written as

$$\frac{\partial V}{\partial t}+\frac{\partial G(V)}{\partial x}=S(V), \tag{2.1}$$

where

$$V=\begin{pmatrix}\rho\\ \rho u\\ \rho p\\ \rho s_x\end{pmatrix},\quad G(V)=\begin{pmatrix}\rho u\\ \rho u^2+p-s_x\\ \rho u p\\ \rho u s_x\end{pmatrix},\quad S(V)=\begin{pmatrix}0\\ 0\\ -K\rho\dot{\varepsilon}_x\\ 4\mu\rho\dot{\varepsilon}_x/3\end{pmatrix}.$$

Here, the variables are, the density ρ, the x-direction velocity u, the hydrostatic pressure p, the x-direction deviatoric stress s_x, the bulk modulus K, the shear modulus μ and the x-direction strain rate $\dot{\varepsilon}_x$. Besides, the hydrostatic pressure and the negative x-direction

https://doi.org/10.4208/aamm.2015.m1340 Published online by Cambridge University Press

deviatoric stress can be merged into one variable, the negative x-direction total stress, expressed by

$$-\sigma = p - s_x. \tag{2.2}$$

Concerning the system (2.1), the first two equations represent the conservation of mass and momentum respectively, while the last two equations denote the Hooke's law in the Eulerian framework interpreted from the following Lagrangian form

$$\dot{p} = K\frac{\dot{\rho}}{\rho}, \quad \dot{s}_x = 2\mu\left(\dot{\varepsilon}_x + \frac{1}{3}\frac{\dot{\rho}}{\rho}\right). \tag{2.3}$$

The dots are time derivatives along the particle path. To facilitate further discussion, conservative formulations (2.1) are rewritten into the non-conservative ones as

$$\begin{cases} \dfrac{\partial \rho}{\partial t} + u\dfrac{\partial \rho}{\partial x} + \rho\dfrac{\partial u}{\partial x} = 0, \\ \dfrac{\partial u}{\partial t} + u\dfrac{\partial u}{\partial x} + \dfrac{1}{\rho}\dfrac{\partial p}{\partial x} - \dfrac{1}{\rho}\dfrac{\partial s_x}{\partial x} = 0, \\ \dfrac{\partial p}{\partial t} + K\dfrac{\partial u}{\partial x} + u\dfrac{\partial p}{\partial x} = 0, \\ \dfrac{\partial s_x}{\partial t} - \dfrac{4}{3}\mu\dfrac{\partial u}{\partial x} + u\dfrac{\partial s_x}{\partial x} = 0. \end{cases} \tag{2.4}$$

2.2 Elastic rarefaction waves

Firstly, we will deduce the relationship across the elastic rarefaction waves. Characteristic speeds of system (2.4) are

$$\lambda_1 = u - \sqrt{\frac{4\mu + 3K}{3\rho}}, \quad \lambda_2 = \lambda_3 = u, \quad \lambda_4 = u + \sqrt{\frac{4\mu + 3K}{3\rho}}. \tag{2.5}$$

For the λ_1-characteristic field, the Riemann invariants across the left rarefaction wave are

$$\begin{cases} I_{\lambda_1}(\rho, u) = u - \sqrt{\dfrac{16\mu + 12K}{3\rho}} = \text{constant}, \\ I_{\lambda_1}(\rho, p) = p - K\ln\rho = \text{constant}, \\ I_{\lambda_1}(\rho, s_x) = s_x + \dfrac{4}{3}\mu\ln\rho = \text{constant}. \end{cases} \tag{2.6}$$

Similarly, for the λ_4-characteristic field, we acquire the Riemann invariants across the right rarefaction wave, given by

$$\begin{cases} I_{\lambda_4}(\rho, u) = u + \sqrt{\dfrac{16\mu + 12K}{3\rho}} = \text{constant}, \\ I_{\lambda_4}(\rho, p) = p - K\ln\rho = \text{constant}, \\ I_{\lambda_4}(\rho, s_x) = s_x + \dfrac{4}{3}\mu\ln\rho = \text{constant}. \end{cases} \tag{2.7}$$

https://doi.org/10.4208/aamm.2015.m1340 Published online by Cambridge University Press

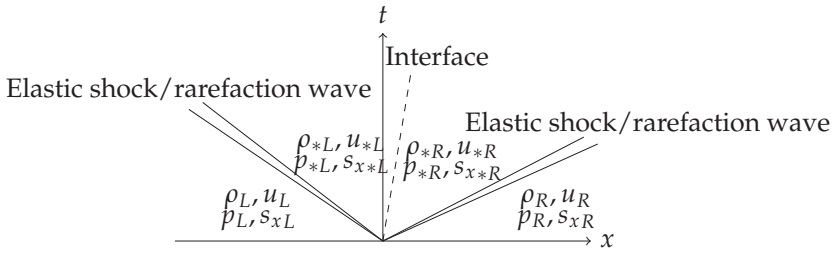


Figure 1: Three-wave solution structure of the elastic solid-solid Riemann problem.

For the λ_1-characteristic field, the relationship of states across the left rarefaction wave can be inferred that

$$u_{*L}=u_L-\sqrt{\frac{16\mu+12K}{3\rho_L}}+\sqrt{\frac{16\mu+12K}{3\rho_{*L}}}, \tag{2.8}$$

together with

$$\frac{\rho_{*L}}{\rho_L}=\exp\Big(\frac{3\sigma_L-3\sigma_{*L}}{3K+4\mu}\Big). \tag{2.9}$$

Similarly, for the λ_4-characteristic field, the relationship of the states across the right rarefaction wave is

$$u_{*R}=u_R+\sqrt{\frac{16\mu+12K}{3\rho_R}}-\sqrt{\frac{16\mu+12K}{3\rho_{*R}}}, \tag{2.10}$$

along with

$$\frac{\rho_{*R}}{\rho_R}=\exp\Big(\frac{3\sigma_R-3\sigma_{*R}}{3K+4\mu}\Big). \tag{2.11}$$

Here, the meanings of above subscripts "L", "$*L$", "$*R$", "R" are the same with the compressible fluid and can be referred to from Fig. 1.

2.3 Elastic shock waves

When the entropy condition is satisfied, elastic shock waves are generated. The Rankine-Hugoniot condition across the elastic shock waves is

$$[\rho u]=S[\rho], \tag{2.12a}$$
$$[\rho u^2-\sigma]=S[\rho u], \tag{2.12b}$$

when applied to the first two equations of system (2.1). Here, "S" stands for the shock wave speed. Therefore, we acquire the formulas

$$u_{*L}=u_L-\sqrt{(\sigma_L-\sigma_{*L})\left(\frac{1}{\rho_L}-\frac{1}{\rho_{*L}}\right)}, \tag{2.13}$$

https://doi.org/10.4208/aamm.2015.m1340 Published online by Cambridge University Press

and

$$u_{*R}=u_R+\sqrt{(\sigma_R-\sigma_{*R})\left(\frac{1}{\rho_R}-\frac{1}{\rho_{*R}}\right)}. \tag{2.14}$$

To associate the densities in front of and behind the shock waves, the Hooke's law Eq. (2.3) is integrated by time t and we have

$$\frac{\rho_{*L}}{\rho_L}=\exp\left(\frac{3\sigma_L-3\sigma_{*L}}{3K+4\mu}\right),\quad \frac{\rho_{*R}}{\rho_R}=\mathrm{Exp}\left(\frac{3\sigma_R-3\sigma_{*R}}{3K+4\mu}\right). \tag{2.15}$$

2.4 The exact elastic solid-solid Riemann solver

Suppose that two parts of the elastic solid are located at the left and right sides of the interface, the one-dimensional elastic solid-solid Riemann problem in the vicinity of the interface can be described in the Euler-Euler coordinate system as

$$\begin{cases} \dfrac{\partial V}{\partial t}+\dfrac{\partial G(V)}{\partial x}=S(V) \quad \text{with } V|_{t=0}=V_L \text{ for } x<x_0, \\ \dfrac{\partial V}{\partial t}+\dfrac{\partial G(V)}{\partial x}=S(V) \quad \text{with } V|_{t=0}=V_R \text{ for } x>x_0, \end{cases} \tag{2.16}$$

where the left constant state V_L and right constant state V_R are separated by the interface located at x_0. Since the λ_2-, λ_3-characteristic fields are linearly degenerate and the λ_1-, λ_4-characteristic fields are genuine non-linear, the exact elastic solid-solid Riemann solution consists of four constant states (V_L,V_{*L},V_{*R},V_R) connected by three elementary waves, where the middle wave associated with the λ_2-, λ_3-characteristic fields is a contact discontinuity and the left and right waves associated with the λ_1-, λ_4-characteristic fields are either shock waves or rarefaction waves, see Fig. 1. To propose the Riemann solver for the elastic solid-solid Riemann problem (2.16), the core strategy is iterating the negative total stress in the star region.

Proposition 2.1. The solution of negative total stress in the star region for the elastic solid-solid Riemann problem (2.16) is given by the root of the algebratic equation

$$h(p_*,W_L,W_R):=g_L|_E(p_*,W_L)+g_R|_E(p_*,W_R)+u_R-u_L=0, \tag{2.17}$$

with

$$p_*=-\sigma_{*L}=-\sigma_{*R},$$

where $g_L|_E(p_*,W_L)$ is given by one of the following two expressions

$$g_L^S|_E(p_*,W_L)=\sqrt{(\sigma_L+p_*)\left(\frac{1}{\rho_L}-\frac{1}{\rho_{*L}}\right)}, \qquad \text{if } \sigma_{*L}<\sigma_L, \tag{2.18a}$$

$$g_L^R|_E(p_*,W_L)=\sqrt{\frac{16\mu+12K}{3\rho_L}}-\sqrt{\frac{16\mu+12K}{3\rho_{*L}}}, \qquad \text{if } \sigma_{*L}\geq\sigma_L, \tag{2.18b}$$

https://doi.org/10.4208/aamm.2015.m1340 Published online by Cambridge University Press

and $g_R|_E(p_*,W_R)$ is given by one of the following two expressions

$$g_R^S|_E(p_*,W_R)=\sqrt{(\sigma_R+p_*)\left(\frac{1}{\rho_R}-\frac{1}{\rho_{*R}}\right)}, \qquad \text{if } \sigma_{*R}<\sigma_R, \tag{2.19a}$$

$$g_R^R|_E(p_{*R},W_R)=\sqrt{\frac{16\mu+12K}{3\rho_R}}-\sqrt{\frac{16\mu+12K}{3\rho_{*R}}}, \qquad \text{if } \sigma_{*R}\geq\sigma_R. \tag{2.19b}$$

The above expressions are enclosed by the corresponding density jump conditions (2.9), (2.11), (2.15). Here, "W" is a vector of primitive variables (ρ,u,p,s_x). Superscripts "S", "R" at the left side of the vertical bar stand for shock wave and rarefaction wave respectively. Subscripts "L", "R" at the left side of the vertical bar denote that the expression is used for the left and right sides of the nonlinear relation respect to the contact discontinuity separately. Subscript "E" at the right side of the vertical bar represents the nonlinear wave is an elastic wave.

To complete the exact Riemann solver, the solution inside the left rarefaction fan is given by

$$W_{Lfan}=\begin{cases} u=\dfrac{2x}{t}-u_L+\sqrt{\dfrac{16\mu+12K}{3\rho_L}}, \\ \rho=\dfrac{4\mu+3K}{3\left(\frac{x}{t}-u_L+\sqrt{\frac{16\mu+12K}{3\rho_L}}\right)^2}, \\ p=p_L-K\ln\rho_L+K\ln\left[\dfrac{4\mu+3K}{3\left(\frac{x}{t}-u_L+\sqrt{\frac{16\mu+12K}{3\rho_L}}\right)^2}\right], \\ s_x=s_{xL}+\dfrac{4}{3}\mu\ln\rho_L-\dfrac{4}{3}\mu\ln\left[\dfrac{4\mu+3K}{3\left(\frac{x}{t}-u_L+\sqrt{\frac{16\mu+12K}{3\rho_L}}\right)^2}\right], \end{cases} \tag{2.20}$$

and the solution inside the right rarefaction fan yields

$$W_{Rfan}=\begin{cases} u=\dfrac{2x}{t}-u_R-\sqrt{\dfrac{16\mu+12K}{3\rho_R}}, \\ \rho=\dfrac{4\mu+3K}{3\left(\frac{x}{t}-u_R-\sqrt{\frac{16\mu+12K}{3\rho_R}}\right)^2}, \\ p=p_R-K\ln\rho_R+K\ln\left[\dfrac{4\mu+3K}{3\left(\frac{x}{t}-u_R-\sqrt{\frac{16\mu+12K}{3\rho_R}}\right)^2}\right], \\ s_x=s_{xR}+\dfrac{4}{3}\mu\ln\rho_R-\dfrac{4}{3}\mu\ln\left[\dfrac{4\mu+3K}{3\left(\frac{x}{t}-u_R-\sqrt{\frac{16\mu+12K}{3\rho_R}}\right)^2}\right], \end{cases} \tag{2.21}$$

assuming that the interface x_0 is located at the original point.

https://doi.org/10.4208/aamm.2015.m1340 Published online by Cambridge University Press

2.5 Solution types of the elastic solid-solid Riemann problem

To determine which expression is expected to be adopted in Eq. (2.17), the solution types have to be classified. In the elastic solid-solid Riemann problem, they are categorized into four types, "$S_E|S_E$", "$S_E|R_E$", "$R_E|S_E$", "$R_E|R_E$". Herein "$|$" means the solid-solid interface, or the contact discontinuity. "S" and "R" indicate that a shock wave or a rarefaction wave is generated at the respective side. Then we have conclusions on the solution types of the elastic solid-solid Riemann problem listed as below.

Lemma 2.1. *Functions* (2.18a), (2.18b), (2.19a), (2.19b) *are differentiable and monotonously increasing with respect to* p_*.

Theorem 2.1. *If the solution type of the elastic solid-solid Riemann problem is "*$S_E|S_E$*", the initial statuses* V_L *and* V_R *satisfy the condition*

$$\begin{aligned} &g_L^S|_E(\max\{-\sigma_L,-\sigma_R\},W_L)+g_R^S|_E(\max\{-\sigma_L,-\sigma_R\},W_R)\\ <&u_L-u_R<g_L^S|_E(+\infty,W_L)+g_R^S|_E(+\infty,W_R). \end{aligned} \tag{2.22}$$

Proof. In this case, elastic shock waves are generated at the both sides according to the initial values V_L and V_R. Hence, functions (2.18a) and (2.19a) are selected for the left side and the right side separately. So Eq. (2.17) becomes

$$h(p_*,W_L,W_R):=g_L^S|_E(p_*,W_L)+g_R^S|_E(p_*,W_R)+u_R-u_L=0.$$

Because of the properties of the left-facing shock wave and the right-facing shock wave, we have $p_*>-\sigma_L$ and $p_*>-\sigma_R$. Thus, the root p_* of the equation lays in the interval $(\max\{-\sigma_L,-\sigma_R\},+\infty)$. As the equation is a monotonously increasing function with respect to p_*, this yields $h(\max\{-\sigma_L,-\sigma_R\},W_L,W_R)<0$ and $h(+\infty,W_L,W_R)>0$, which are

$$g_L^S|_E(\max\{-\sigma_L,-\sigma_R\},W_L)+g_R^S|_E(\max\{-\sigma_L,-\sigma_R\},W_R)+u_R-u_L<0,$$

and

$$g_L^S|_E(+\infty,W_L)+g_R^S|_E(+\infty,W_R)+u_R-u_L>0.$$

Thus, we complete the proof. □

Similarly, the following theorems can be proved.

Theorem 2.2. *If the solution type of the elastic solid-solid Riemann problem is "*$S_E|R_E$*", the initial statuses* V_L *and* V_R *satisfy the condition*

$$g_L^S|_E(-\sigma_L,W_L)+g_R^R|_E(-\sigma_L,W_R)<u_L-u_R\le g_L^S|_E(-\sigma_R,W_L)+g_R^R|_E(-\sigma_R,W_R). \tag{2.23}$$

Theorem 2.3. *If the solution type of the elastic solid-solid Riemann problem is "*$R_E|S_E$*", the initial statuses* V_L *and* V_R *satisfy the condition*

$$g_L^R|_E(-\sigma_R,W_L)+g_R^S|_E(-\sigma_R,W_R)<u_L-u_R\le g_L^R|_E(-\sigma_L,W_L)+g_R^S|_E(-\sigma_L,W_R). \tag{2.24}$$

https://doi.org/10.4208/aamm.2015.m1340 Published online by Cambridge University Press

Theorem 2.4. *If the solution type of the elastic solid-solid Riemann problem is "$R_E|R_E$", the initial statuses V_L and V_R satisfy the condition*

$$\begin{aligned}&g_L^R|_E(0,W_L)+g_R^R|_E(0,W_R)\\ \leq& u_L-u_R\\ \leq& g_L^R|_E(\min\{-\sigma_L,-\sigma_R\},W_L)+g_R^R|_E(\min\{-\sigma_L,-\sigma_R\},W_R).\end{aligned} \tag{2.25}$$

3 The perfectly plastic waves and the exact perfectly plastic solid-solid Riemann solver

In this part, the perfectly plastic rarefaction wave and shock wave are analysed and the exact perfectly plastic solid-solid Riemann solver is proposed dismissing the effect of elasticity.

3.1 Governing equations and constitutive models for the perfectly plastic solid

Ignoring the effects of body forces, viscous stresses and heat-conducting, the one-dimensional non-linear system of hyperbolic conservation laws in the Eulerian coordinate system to express the perfectly plastic solid is given by

$$\frac{\partial V}{\partial t}+\frac{\partial G(V)}{\partial x}=0, \tag{3.1}$$

where

$$V=\begin{pmatrix}\rho\\ \rho u\\ E\end{pmatrix},\quad G(V)=\begin{pmatrix}\rho u\\ \rho u^2+p-s_x\\ (E+p-s_x)u\end{pmatrix}.$$

Herein the deviatoric stress s_x is treated as a constant owing to the perfectly plastic assumption and E is the total energy per unit volume, which is defined by

$$E=\frac{1}{2}\rho u^2+\rho e, \tag{3.2}$$

where e is the specific internal energy. For closure of the system (3.1), equation of state is required. In this study, the solid is assumed to equip with the "stiffened-gas" equation of state associating with the hydrostatic pressure p through

$$p(\rho,e)=c_0^2(\rho-\rho_0)+(\gamma-1)\rho e. \tag{3.3}$$

In the above equation, c_0 is the unshocked sound speed, ρ_0 is the reference density, and γ is the Grüneisen gamma. As a result, the non-conservation formulations for the one-

https://doi.org/10.4208/aamm.2015.m1340 Published online by Cambridge University Press

dimensional perfectly plastic solid is written as

$$\begin{cases} \dfrac{\partial \rho}{\partial t}+u\dfrac{\partial \rho}{\partial x}+\rho\dfrac{\partial u}{\partial x}=0, \\ \dfrac{\partial u}{\partial t}+u\dfrac{\partial u}{\partial x}+\dfrac{1}{\rho}\dfrac{\partial p}{\partial x}=0, \\ \dfrac{\partial p}{\partial t}+[\rho a^2-(\gamma-1)s_x]\dfrac{\partial u}{\partial x}+u\dfrac{\partial p}{\partial x}=0, \end{cases} \tag{3.4}$$

where a is a variable and equals to $\sqrt{(\gamma p+c_0^2\rho_0)/\rho}$.

3.2 Rarefaction waves

Considering the rarefaction waves in the perfectly plastic solid, the characteristic speeds of system (3.4) are

$$\lambda_1=u-\sqrt{a^2-\frac{(\gamma-1)s_x}{\rho}},\quad \lambda_2=u,\quad \lambda_3=u+\sqrt{a^2-\frac{(\gamma-1)s_x}{\rho}}. \tag{3.5}$$

For the λ_1-characteristic field, the Riemann invariants across the left rarefaction wave are given by

$$\begin{cases} I_L(\rho,u)=u+\displaystyle\int\frac{1}{\rho}\sqrt{a^2-\frac{(\gamma-1)s_x}{\rho}}d\rho=\text{constant}, \\ I_L(\rho,p)=\dfrac{1}{\gamma}\ln[\gamma p+c_0^2\rho_0-(\gamma-1)s_x]-\ln\rho=\text{constant}. \end{cases} \tag{3.6}$$

Similarly, for the λ_3-characteristic field, the Riemann invariants across the right rarefaction wave are

$$\begin{cases} I_R(\rho,u)=u-\displaystyle\int\frac{1}{\rho}\sqrt{a^2-\frac{(\gamma-1)s_x}{\rho}}d\rho=\text{constant}, \\ I_R(\rho,p)=\dfrac{1}{\gamma}\ln[\gamma p+c_0^2\rho_0-(\gamma-1)s_x]-\ln\rho=\text{constant}. \end{cases} \tag{3.7}$$

The integral terms in Eqs. (3.6) and (3.7) can be calculated by numerical integration method or expended as the following Taylor series

$$\int\frac{1}{\rho}\sqrt{a^2-\frac{(\gamma-1)s_x}{\rho}}d\rho\approx\frac{2a}{\gamma-1}+\frac{(\gamma-1)s_x}{(\gamma+1)\rho a}+\frac{1}{4}\frac{(\gamma-1)^2s_x^2}{3\gamma+1}\frac{1}{\rho^2a^3}+\cdots. \tag{3.8}$$

If we truncate the first two terms, the truncation error can be estimated by

$$|R_2(x)|=\left|\int\frac{f''(\theta)}{2!}\frac{(\gamma-1)^2s_x^2}{\rho^3a^3}d\rho\right|<\frac{(\gamma-1)^2}{3\gamma+1}\frac{s_x^2}{\rho^2a^3},\quad 0<\theta\le\frac{(\gamma-1)s_x}{c_0^2\rho_0}, \tag{3.9}$$

https://doi.org/10.4208/aamm.2015.m1340 Published online by Cambridge University Press

where $f''(x)=-(1-x)^{-\frac{3}{2}}/4$. After the truncation, the relationship of states across the left plastic rarefaction wave can be inferred that

$$u_{*L}=u_L-\frac{2a_L}{\gamma-1}\left[\left(\frac{p_{*L}+\frac{c_0^2\rho_0-(\gamma-1)s_{x*L}}{\gamma}}{p_L+\frac{c_0^2\rho_0-(\gamma-1)s_{xL}}{\gamma}}\right)^{\frac{\gamma-1}{2\gamma}}-1\right], \tag{3.10}$$

together with

$$\frac{\rho_{*L}}{\rho_L}=\left(\frac{p_{*L}+\frac{c_0^2\rho_0-(\gamma-1)s_{x*L}}{\gamma}}{p_L+\frac{c_0^2\rho_0-(\gamma-1)s_{xL}}{\gamma}}\right)^{\frac{1}{\gamma}}. \tag{3.11}$$

For the right plastic rarefaction wave, the counterpart formula is

$$u_{*R}=u_R+\frac{2a_R}{\gamma-1}\left[\left(\frac{p_{*R}+\frac{c_0^2\rho_0-(\gamma-1)s_{x*R}}{\gamma}}{p_R+\frac{c_0^2\rho_0-(\gamma-1)s_{xR}}{\gamma}}\right)^{\frac{\gamma-1}{2\gamma}}-1\right], \tag{3.12}$$

along with

$$\frac{\rho_{*R}}{\rho_R}=\left(\frac{p_{*R}+\frac{c_0^2\rho_0-(\gamma-1)s_{x*R}}{\gamma}}{p_R+\frac{c_0^2\rho_0-(\gamma-1)s_{xR}}{\gamma}}\right)^{\frac{1}{\gamma}}. \tag{3.13}$$

3.3 Shock waves

When the entropy condition is satisfied, the Rankine-Hugoniot condition is applied to the system (3.1) and we obtain

$$[\rho u]=S[\rho], \tag{3.14a}$$
$$[\rho u^2-\sigma]=S[\rho u], \tag{3.14b}$$
$$[(E-\sigma)u]=S[E]. \tag{3.14c}$$

Then the equations across the plastic shock waves derived from the above three jump conditions yield

$$u_{*L}=u_L-\sqrt{(\sigma_L-\sigma_{*L})\left(\frac{1}{\rho_L}-\frac{1}{\rho_{*L}}\right)}, \tag{3.15a}$$

$$u_{*R}=u_R+\sqrt{(\sigma_R-\sigma_{*R})\left(\frac{1}{\rho_R}-\frac{1}{\rho_{*R}}\right)}, \tag{3.15b}$$

https://doi.org/10.4208/aamm.2015.m1340 Published online by Cambridge University Press

where the density jumps across the plastic shock waves are given by

$$\frac{\rho_{*L}}{\rho_L}=\frac{(\gamma-1)\sigma_{*L}+(\gamma-1)\sigma_L-2p_{*L}-2c_0^2\rho_0}{(\gamma-1)\sigma_L+(\gamma-1)\sigma_{*L}-2p_L-2c_0^2\rho_0}, \tag{3.16a}$$

$$\frac{\rho_{*R}}{\rho_R}=\frac{(\gamma-1)\sigma_{*R}+(\gamma-1)\sigma_R-2p_{*R}-2c_0^2\rho_0}{(\gamma-1)\sigma_R+(\gamma-1)\sigma_{*R}-2p_R-2c_0^2\rho_0}. \tag{3.16b}$$

3.4 The exact perfectly plastic solid-solid Riemann solver

Suppose that two pieces of the perfectly plastic solid are located at the left and right sides of the interface respectively, thus the one-dimensional perfectly plastic solid-solid Riemann problem in the vicinity of the interface can be described in the Euler-Euler coordinate system as

$$\begin{cases} \dfrac{\partial V}{\partial t}+\dfrac{\partial G(V)}{\partial x}=0 \quad \text{with } V|_{t=0}=V_L \text{ for } x<x_0, \\ \dfrac{\partial V}{\partial t}+\dfrac{\partial G(V)}{\partial x}=0 \quad \text{with } V|_{t=0}=V_R \text{ for } x>x_0. \end{cases} \tag{3.17}$$

Since the λ_2-characteristic field is linearly degenerate and the λ_1-, λ_3-characteristic fields are genuine non-linear, the exact perfectly plastic solid-solid Riemann solution consists of four constant states (V_L,V_{*L},V_{*R},V_R) connected by three elementary waves, where the middle wave associated with the λ_2-characteristic field is a contact discontinuity and the left and right waves associated with the λ_1-, λ_3-characteristic fields are either shock waves or rarefaction waves, see Fig. 2. To propose the Riemann solver for the perfectly plastic solid-solid Riemann problem (3.17), the core strategy is iterating the negative total stress in the star region.

Proposition 3.1. The solution of negative total stress in the star region for the perfectly plastic solid-solid Riemann problem (3.17) is given by the root of the algebratic equation

$$h(p_*,W_L,W_R):=g_L|_P(p_*,W_L)+g_R|_P(p_*,W_R)+u_R-u_L=0, \tag{3.18}$$

with

$$p_*=-\sigma_{*L}=-\sigma_{*R},$$

where $g_L|_P(p_*,W_L)$ is given by one of the following two expressions

$$g_L^S|_P(p_*,W_L)=\sqrt{(\sigma_L+p_*)\left(\frac{1}{\rho_L}-\frac{1}{\rho_{*L}}\right)}, \qquad \text{if } \sigma_{*L}<\sigma_L, \tag{3.19a}$$

$$g_L^R|_P(p_*,W_L)=\frac{2a_L}{\gamma-1}\left[\left(\frac{p_{*L}+\frac{c_0^2\rho_0-(\gamma-1)s_{x*L}}{\gamma}}{p_L+\frac{c_0^2\rho_0-(\gamma-1)s_{xL}}{\gamma}}\right)^{\frac{\gamma-1}{2\gamma}}-1\right], \qquad \text{if } \sigma_{*L}\geq\sigma_L, \tag{3.19b}$$

https://doi.org/10.4208/aamm.2015.m1340 Published online by Cambridge University Press

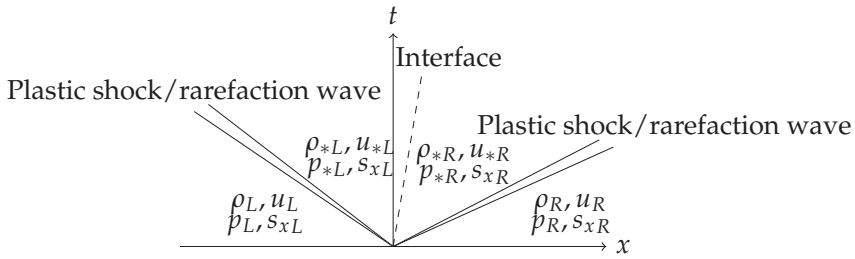


Figure 2: Three-wave solution structure of the perfectly plastic solid-solid Riemann problem.

and $g_R|_P(p_*, W_R)$ is given by one of the following two expressions

$$g_R^S|_P(p_*, W_R) = \sqrt{(\sigma_R + p_*)\left(\frac{1}{\rho_R} - \frac{1}{\rho_{*R}}\right)}, \qquad \text{if } \sigma_{*R} < \sigma_R, \tag{3.20a}$$

$$g_R^R|_P(p_*, W_R) = \frac{2a_R}{\gamma - 1}\left[\left(\frac{p_{*R} + \frac{c_0^2\rho_0 - (\gamma-1)s_{x*R}}{\gamma}}{p_R + \frac{c_0^2\rho_0 - (\gamma-1)s_{xR}}{\gamma}}\right)^{\frac{\gamma-1}{2\gamma}} - 1\right], \qquad \text{if } \sigma_{*R} \geq \sigma_R. \tag{3.20b}$$

The above expressions are enclosed by the corresponding density jump conditions (3.11), (3.13), (3.16a), (3.16b). Here, subscript "P" at the right side of the vertical bar represents the nonlinear wave is a plastic wave.

If the interface x_0 is located at the original point, the solution inside the left rarefaction fan is given by

$$W_{Lfan} = \begin{cases} \rho = \left[\dfrac{\left(u_L - \frac{x}{t}\right)^2 \rho_L^{\gamma+1}}{\gamma p_L + c_0^2\rho_0 - (\gamma-1)s_{xL}}\right]^{\frac{1}{\gamma+1}}, \\ u = \dfrac{x}{t} + \left(u_L - \dfrac{x}{t}\right)\dfrac{\rho_L}{\rho}, \\ p = \dfrac{1}{\gamma}\left[\left(u_L - \dfrac{x}{t}\right)^2 \dfrac{\rho_L^2}{\rho} + (\gamma-1)s_{xL} - c_0^2\rho_0\right], \end{cases} \tag{3.21}$$

and the solution inside the right rarefaction fan yields

$$W_{Rfan} = \begin{cases} \rho = \left[\dfrac{\left(u_R - \frac{x}{t}\right)^2 \rho_L^{\gamma+1}}{\gamma p_R + c_0^2\rho_0 - (\gamma-1)s_{xR}}\right]^{\frac{1}{\gamma+1}}, \\ u = \dfrac{x}{t} + \left(u_R - \dfrac{x}{t}\right)\dfrac{\rho_R}{\rho}, \\ p = \frac{1}{\gamma}\left[\left(u_R - \dfrac{x}{t}\right)^2 \dfrac{\rho_R^2}{\rho} + (\gamma-1)s_{xR} - c_0^2\rho_0\right]. \end{cases} \tag{3.22}$$

https://doi.org/10.4208/aamm.2015.m1340 Published online by Cambridge University Press

3.5 Solution types of the perfectly plastic solid-solid Riemann problem

Similar to the content discussed in subsection 2.5, for this perfectly plastic solid-solid Riemann problem, the solution types are also categorized into four types, "$S_P|S_P$", "$S_P|R_P$", "$R_P|S_P$", "$R_P|R_P$". Then we have conclusions listed as below.

Lemma 3.1. *Functions* (3.19a), (3.19b), (3.20a), (3.20b) *are differentiable and monotonously increasing with respect to* p_*.

Theorem 3.1. *If the solution type of the perfectly plastic solid-solid Riemann problem is "*$S_P|S_P$*", the initial statuses* V_L *and* V_R *satisfy the condition*

$$\begin{aligned} &g_L^S|_P(\max\{-\sigma_L,-\sigma_R\},W_L)+g_R^S|_P(\max\{-\sigma_L,-\sigma_R\},W_R)\\ <&u_L-u_R<g_L^S|_P(+\infty,W_L)+g_R^S|_P(+\infty,W_R). \end{aligned} \tag{3.23}$$

Theorem 3.2. *If the solution type of the perfectly plastic solid-solid Riemann problem is "*$S_P|R_P$*", the initial statuses* V_L *and* V_R *satisfy the condition*

$$g_L^S|_P(-\sigma_L,W_L)+g_R^R|_P(-\sigma_L,W_R)<u_L-u_R\leq g_L^S|_P(-\sigma_R,W_L)+g_R^R|_P(-\sigma_R,W_R). \tag{3.24}$$

Theorem 3.3. *If the solution type of the perfectly plastic solid-solid Riemann problem is "*$R_P|S_P$*", the initial statuses* V_L *and* V_R *satisfy the condition*

$$g_L^R|_P(-\sigma_R,W_L)+g_R^S|_P(-\sigma_R,W_R)<u_L-u_R\leq g_L^R|_P(-\sigma_L,W_L)+g_R^S|_P(-\sigma_L,W_R). \tag{3.25}$$

Theorem 3.4. *If the solution type of the perfectly plastic solid-solid Riemann problem is "*$R_P|R_P$*", the initial statuses* V_L *and* V_R *satisfy the condition*

$$\begin{aligned} &g_L^R|_P(0,W_L)+g_R^R|_P(0,W_R)\\ \leq&u_L-u_R\\ \leq&g_L^R|_P(\min\{-\sigma_L,-\sigma_R\},W_L)+g_R^R|_P(\min\{-\sigma_L,-\sigma_R\},W_R). \end{aligned} \tag{3.26}$$

4 The exact elastic-perfectly plastic solid-solid Riemann solver

4.1 Governing equations and constitutive models for the elastic-perfectly plastic solid

The one-dimensional governing equations for the elastic-perfectly plastic solid remain to be system (3.1), but the deviatoric stress s_x acts as a variable. In addition, the von Mises yield condition is imposed to judge the material status at a particular point. The solid is in the elastic region if the von Mises yield condition is satisfied, in terms of deviatoric stress, which is

$$s_x^2\leq\left(\frac{2}{3}Y_0\right)^2. \tag{4.1}$$

https://doi.org/10.4208/aamm.2015.m1340 Published online by Cambridge University Press

Here, Y_0 is the yield strength of the material in simple tension. And Hooke's law (2.3) is used to describe the elastic material. Otherwise, when the inequality (4.1) is violated, perfectly plastic flow occurs and the deviatoric component s_x is assume to remain constant in the plastic region, namely

$$s_x = \pm\frac{2}{3}Y_0. \tag{4.2}$$

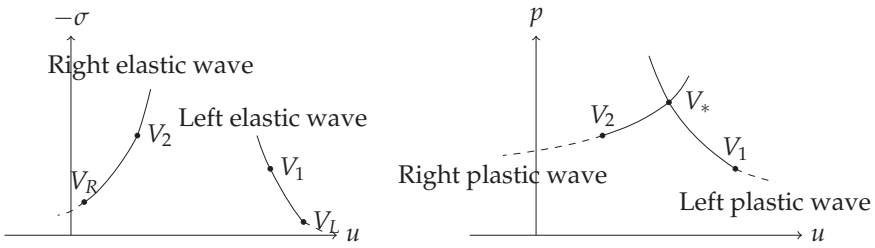
Note that the material yields in tension if $s_x > 0$ and in compression if $s_x < 0$. The hydrostatic pressure can be negative but it is cut off at $-Y_0/3$. In summary, the compete elastic-perfectly plastic solid constitutive model in one dimension is demonstrated as

$$\begin{cases} \text{(I) The negative total stress decomposition: } -\sigma = p - s_x, \\ \text{(II) The von Mises yield condition: } s_x^2 \le \left(\frac{2}{3}Y_0\right)^2, \\ \text{(III) The Hooke's law: } \dot{p} = K\frac{\dot{\rho}}{\rho}, \quad \dot{s}_x = 2\mu\left(\dot{\varepsilon}_x + \frac{1}{3}\frac{\dot{\rho}}{\rho}\right), \\ \text{(IV) The perfectly plastic assumption: } s_x = \pm\frac{2}{3}Y_0, \\ \text{(V) The stiffened-gas equation of state: } p = p(\rho,e), \\ \text{(VI) The minimized hydrostatic pressure: } \min p = -\frac{1}{3}Y_0. \end{cases} \tag{4.3}$$

4.2 The elastic-plastic phase transition

When the solid undergoes the elastic-plastic phase transition, its constitutive model is distinguished by the elastic limit. We define the states of the elastic limit within the left and right sides of the solid as V_1 and V_2. As a single wave is insufficient to connect the initial state with the star region state owing to the different constitutive models at the elastic region and the perfectly plastic region, the wave structure has to be split into two segments, the elastic wave that links the initial state to the elastic limit state and the plastic wave that connects the elastic limit state with the star region state. The phase planes help us illustrate the solution structure of the elastic-perfectly plastic Riemann problem. As shown in Fig. 3(a), we project the Hugoniot loci and integral curves for the elastic waves from four dimensional (ρ,u,p,s_x) phase space into two dimensional $(-\sigma,u)$ phase space onto this plane. Hence, there exists an elastic wave passing from V_L to V_1, so does an elastic wave passing from V_R to V_2. In this example, the states are connected by elastic shock waves depicted in solid lines, while the dashed lines indicate the links are elastic rarefaction waves. For Fig. 3(b), because the deviatoric stress s_x is a constant in the plastic region, the Hugoniot loci and integral curves for plastic waves are projected from three dimensional (ρ,u,p) phase space into two dimensional (p,u) phase space onto this plane. The new state V_* merge as an intersection of two plastic waves. Finally, if two sides of the elastic-perfectly plastic solid undergo the elastic-plastic phase transition, the solution structure of its Riemann problem can be drawn as Fig. 4.

https://doi.org/10.4208/aamm.2015.m1340 Published online by Cambridge University Press



(a) The elastic wave phase plane (b) The plastic wave phase plane

Figure 3: The phase plane of elastic-perfectly plastic solid-solid Riemann problem with elastic-plastic phase transition.

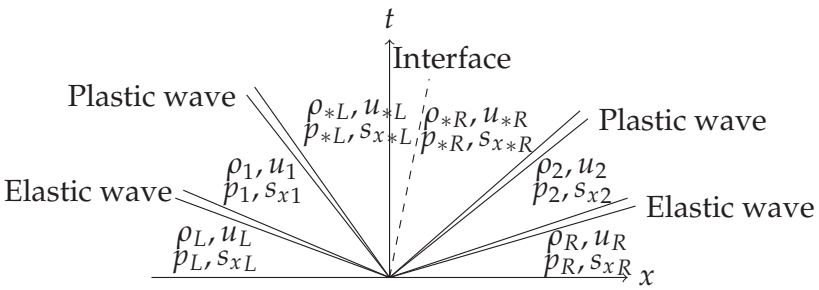


Figure 4: Five-wave solution structure of the elastic-perfectly plastic solid-solid Riemann problem.

4.3 The elastic limit state

Integrating the Hooke's law by time and associating it with the von Mises criterion, we can compute the values of the elastic limit state.

Proposition 4.1. When the solid undergoes elastic up to perfectly plastic compression, the hydrostatic pressure and deviatoric stress at the elastic limit state V_1 and V_2 are given by

$$\begin{cases} p_{1C} = p_L + K\dfrac{2Y_0 + 3s_{xL}}{4\mu}, & s_{x1C} = -\dfrac{2}{3}Y_0, \\ p_{2C} = p_R + K\dfrac{2Y_0 + 3s_{xR}}{4\mu}, & s_{x2C} = -\dfrac{2}{3}Y_0. \end{cases} \tag{4.4}$$

Proposition 4.2. When the solid undergoes elastic up to perfectly plastic tension, the hydrostatic pressure and deviatoric stress at the elastic limit state V_1 and V_2 are given by

$$\begin{cases} p_{1T} = p_L - K\dfrac{2Y_0 - 3s_{xL}}{4\mu}, & s_{x1T} = \dfrac{2}{3}Y_0, \\ p_{2T} = p_R - K\dfrac{2Y_0 - 3s_{xR}}{4\mu}, & s_{x2T} = \dfrac{2}{3}Y_0. \end{cases} \tag{4.5}$$

Here, appended subscripts "C" and "T" are short for "Compression" and "Tension".

https://doi.org/10.4208/aamm.2015.m1340 Published online by Cambridge University Press

4.4 The exact five-wave elastic-perfectly plastic solid-solid Riemann solver

Suppose that two parts of the elastic-perfectly plastic solid are located at the left and right sides of the interface respectively and they both undergo the elastic-plastic phase transition, the one-dimensional elastic-perfectly plastic solid-solid Riemann problem in the vicinity of the interface can be described in the Euler-Euler coordinate system as

$$\begin{cases} \dfrac{\partial V}{\partial t}+\dfrac{\partial G(V)}{\partial x}=0 \quad \text{with} \quad V|_{t=0}=V_L \quad \text{for } x<x_0, \\ \dfrac{\partial V}{\partial t}+\dfrac{\partial G(V)}{\partial x}=0 \quad \text{with} \quad V|_{t=0}=V_R \quad \text{for } x>x_0. \end{cases} \tag{4.6}$$

Following the conclusion discussed in Subsection 4.2, the exact solution consists of six constant states $(V_L,V_1,V_{*L},V_{*R},V_2,V_R)$ connected by five elementary waves (see Fig. 4), where the middle wave is a contact discontinuity and the left and right waves are either shock waves or rarefaction waves of the same type [26]. To propose the Riemann solver for the elastic-perfectly plastic solid-solid Riemann problem (4.6), the core strategy is iterating the negative total stress in the star region.

Proposition 4.3. The solution of negative total stress in the star region for the elastic-perfectly plastic solid-solid Riemann problem (4.6) is given by the root of the algebratic equation

$$h(p_*,W_L,W_R):=g_L|_{EP}(p_*,W_L)+g_R|_{PE}(p_*,W_R)+u_R-u_L=0, \tag{4.7}$$

with

$$p_*=-\sigma_{*L}=-\sigma_{*R},$$

where $g_L|_{EP}(p_*,W_L)$ is given by one of the following two expressions

$$\begin{aligned} g_L^S|_{EP}(p_*,W_L)=&\sqrt{(\sigma_L-\sigma_{1C})\left(\frac{1}{\rho_L}-\frac{1}{\rho_{1C}}\right)} \\ &+\sqrt{(\sigma_{1C}+p_*)\left(\frac{1}{\rho_{1C}}-\frac{1}{\rho_{*L}}\right)}, \qquad \sigma_{*L}<\sigma_{1C}<\sigma_L, \end{aligned} \tag{4.8a}$$

$$\begin{aligned} g_L^R|_{EP}(p_*,W_L)=&\frac{2a_{1T}}{\gamma-1}\left[\left(\frac{p_{*L}+\frac{c_0^2\rho_0-(\gamma-1)s_{x*L}}{\gamma}}{p_{1T}+\frac{c_0^2\rho_0-(\gamma-1)s_{xL}}{\gamma}}\right)^{\frac{\gamma-1}{2\gamma}}-1\right] \\ &+\sqrt{\frac{16\mu+12K}{3\rho_L}}-\sqrt{\frac{16\mu+12K}{3\rho_{1T}}}, \qquad \sigma_{*L}\geq\sigma_{1T}\geq\sigma_L, \end{aligned} \tag{4.8b}$$

https://doi.org/10.4208/aamm.2015.m1340 Published online by Cambridge University Press

and $g_R|_{PE}(p_*,W_R)$ is given by one of the following two expressions

$$g_R^S|_{PE}(p_*,W_R)=\sqrt{(\sigma_{2C}+p_*)\left(\frac{1}{\rho_{2C}}-\frac{1}{\rho_{*R}}\right)}+\sqrt{(\sigma_R-\sigma_{2C})\left(\frac{1}{\rho_R}-\frac{1}{\rho_{2C}}\right)}, \qquad \sigma_{*R}<\sigma_{2C}<\sigma_R, \tag{4.9a}$$

$$g_R^R|_{PE}(p_*,W_R)=\frac{2a_{2T}}{\gamma-1}\left[\left(\frac{p_{*R}+\frac{c_0^2\rho_0-(\gamma-1)s_{x*R}}{\gamma}}{p_{2T}+\frac{c_0^2\rho_0-(\gamma-1)s_{xR}}{\gamma}}\right)^{\frac{\gamma-1}{2\gamma}}-1\right]+\sqrt{\frac{16\mu+12K}{3\rho_R}}-\sqrt{\frac{16\mu+12K}{3\rho_{2T}}}, \qquad \sigma_{*R}\geq\sigma_{2T}\geq\sigma_R. \tag{4.9b}$$

The above expressions are enclosed by the corresponding density jump conditions (2.9), (2.11), (2.15), (3.11), (3.13), (3.16a), (3.16b). Subscripts "EP" and "PE" at the right side of the vertical bar represent the nonlinear waves are the combination of elastic wave and plastic wave. It is need to be mentioned that any iterative method for solving the nonlinear equation (4.7) can be employed. In this work, to make sure the robustness of the Riemann solver, we adopt the bisection method.

4.5 Solution types of the five-wave elastic-perfectly plastic solid-solid Riemann problem

For the elastic-perfectly plastic solid-solid Riemann problem, the five-wave structured solutions are categorized into four types, "$S_ES_P|S_PS_E$", "$S_ES_P|R_PR_E$", "$R_ER_P|S_PS_E$", "$R_ER_P|R_PR_E$". Their corresponding theorems are listed as below.

Lemma 4.1. *Functions* (4.8a), (4.8b), (4.9a), (4.10) *are differentiable and monotonously increasing with respect to* p_*.

Theorem 4.1. *If the solution type of the elastic-perfectly plastic solid-solid Riemann problem is "$S_ES_P|S_PS_E$", the initial statuses V_L and V_R satisfy the auxiliary condition $s_{xL}\neq s_{x1C}$, $s_{xR}\neq s_{x2C}$ and the inequalities*

$$\begin{aligned}&g_L^S|_{EP}(\max\{-\sigma_1,-\sigma_2\},W_L)+g_R^S|_{PE}(\max\{-\sigma_1,-\sigma_2\},W_R)\\<&u_L-u_R<g_L^S|_{EP}(+\infty,W_L)+g_R^S|_{PE}(+\infty,W_R).\end{aligned} \tag{4.10}$$

Theorem 4.2. *If the solution type of the elastic-perfectly plastic solid-solid Riemann problem is "$S_ES_P|R_PR_E$", the initial statuses V_L and V_R satisfy the auxiliary condition $s_{xL}\neq s_{x1C}$, $s_{xR}\neq s_{x2T}$ and the inequalities*

$$g_L^S|_{EP}(-\sigma_1,W_L)+g_R^R|_{EP}(-\sigma_1,W_R)<u_L-u_R\leq g_L^S|_{EP}(-\sigma_2,W_L)+g_R^R|_{EP}(-\sigma_2,W_R). \tag{4.11}$$

https://doi.org/10.4208/aamm.2015.m1340 Published online by Cambridge University Press

Theorem 4.3. *If the solution type of the elastic-perfectly plastic solid-solid Riemann problem is "$R_ER_P|S_PS_E$", the initial statuses V_L and V_R satisfy the auxiliary condition $s_{xL}\neq s_{x1T}$, $s_{xR}\neq s_{x2C}$ and the inequalities*

$$g_L^R|_{EP}(-\sigma_2,W_L)+g_R^S|_{EP}(-\sigma_2,W_R)<u_L-u_R\leq g_L^R|_{EP}(-\sigma_1,W_L)+g_R^S|_{EP}(-\sigma_1,W_R). \quad (4.12)$$

Theorem 4.4. *If the solution type of the elastic-perfectly plastic solid-solid Riemann problem is "$R_ER_P|R_PR_E$", the initial statuses V_L and V_R satisfy the auxiliary condition $s_{xL}\neq s_{x1T}$, $s_{xR}\neq s_{x2T}$ and the inequalities*

$$\begin{aligned}&g_L^R|_{EP}(-Y_0,W_L)+g_R^R|_{PE}(-Y_0,W_R)\\ \leq&u_L-u_R\leq g_L^R|_{EP}(\min\{-\sigma_1,-\sigma_2\},W_L)+g_R^R|_{PR}(\min\{-\sigma_1,-\sigma_2\},W_R).\end{aligned} \quad (4.13)$$

Among the above theorems, the auxiliary condition is an additional condition to guarantee the generation of elastic waves.

4.6 The complete exact elastic-perfectly plastic solid-solid Riemann solver

If neither side undergoes the elastic-plastic phase transition, the solution is a three-wave structure. Only one nonlinear wave is generated at the both sides. In this circumstance, solution types include $S_E|S_E$, $S_E|R_E$, $R_E|S_E$, $R_E|R_E$, $S_P|S_P$, $S_P|R_P$, $R_P|S_P$, $R_P|R_P$, $S_E|S_P$, $S_E|R_P$, $R_E|S_P$, $R_E|R_P$, $S_P|S_E$, $S_P|R_E$, $R_P|S_E$, $R_P|R_E$. If only one side undergoes the elastic-plastic phase transition, the solution is a four-wave structure. One nonlinear wave is generated at one side while two nonlinear waves are generated at the other side. In this case, solution types include $S_E|S_PS_E$, $S_E|R_PR_E$, $R_E|S_PS_E$, $R_E|R_PR_E$, $S_P|S_PS_E$, $S_P|R_PR_E$, $R_P|S_PS_E$, $R_P|R_PR_E$, $S_ES_P|S_E$, $S_ES_P|R_E$, $R_ER_P|S_E$, $R_ER_P|R_E$, $S_ES_P|S_P$, $S_ES_P|R_P$, $R_ER_P|S_P$, $R_ER_P|R_P$. The corresponding exact Riemann solvers for these thirty-two solution types can be acquired by referring to the Proposition 4.3. Given that the initial states have been provided, as for which solution type is true, it can be searched one by one as listed in the Table 1, judging by its auxiliary condition and solution interval which the exact solution has to be in. Therefore, the integral Riemann solvers for these thirty-six solution types form the complete exact elastic-perfectly plastic solid-solid Riemann solver.

5 Numerical justifications of the exact solid Riemann solvers

The correctness of the above exact Riemann solvers can be verified by comparing the results with the outcomes computed by the ordinary finite-difference scheme. In the following justifications, the scheme is conducted by the Lax-Friedrichs scheme. Besides, for the Lax-Friedrichs scheme, given that the time level is n and there are M uniform grid points, the maximum sound speed can be estimated by

$$S_{\max}^n=\max_i\{|u_i^n|+c_i^n\},\quad i=1,2,\cdots,M, \quad (5.1)$$

https://doi.org/10.4208/aamm.2015.m1340 Published online by Cambridge University Press

Table 1: Auxiliary condition and solution interval of each solution type for the complete exact elastic-perfectly plastic solid-solid Riemann solver.

Solution type	Auxiliary condition	Solution interval
$S_E\|S_E$	$s_{xL}\neq s_{x1C}, s_{xR}\neq s_{x2C}$	$(\max\{-\sigma_L,-\sigma_R\},\min\{-\sigma_{1C},-\sigma_{2C}\})$
$S_E\|R_E$	$s_{xL}\neq s_{x1C}, s_{xR}\neq s_{x2T}$	$(\max\{-\sigma_L,-\sigma_{2T}\},\min\{-\sigma_R,-\sigma_{1C}\}]$
$R_E\|S_E$	$s_{xL}\neq s_{x1T}, s_{xR}\neq s_{x2C}$	$(\max\{-\sigma_R,-\sigma_{1T}\},\min\{-\sigma_L,-\sigma_{2C}\}]$
$R_E\|R_E$	$s_{xL}\neq s_{x1T}, s_{xR}\neq s_{x2T}$	$[\max\{-\sigma_{1T},-\sigma_{2T}\},\min\{-\sigma_L,-\sigma_R\}]$
$S_P\|S_P$	$s_{xL}= s_{x1C}, s_{xR}= s_{x2C}$	$(\max\{-\sigma_L,-\sigma_R\},+\infty)$
$S_P\|R_P$	$s_{xL}= s_{x1C}, s_{xR}= s_{x2T}$	$(-\sigma_L,-\sigma_R]$
$R_P\|S_P$	$s_{xL}= s_{x1T}, s_{xR}= s_{x2C}$	$(-\sigma_R,-\sigma_L]$
$R_P\|R_P$	$s_{xL}= s_{x1T}, s_{xR}= s_{x2T}$	$[-Y_0,\min\{-\sigma_L,-\sigma_R\}]$
$S_E\|S_P$	$s_{xL}\neq s_{x1C}, s_{xR}= s_{x2C}$	$(\max\{-\sigma_L,-\sigma_R\},-\sigma_{1C})$
$S_E\|R_P$	$s_{xL}\neq s_{x1C}, s_{xR}= s_{x2T}$	$(-\sigma_L,\min\{-\sigma_{1C},-\sigma_R\}]$
$R_E\|S_P$	$s_{xL}\neq s_{x1T}, s_{xR}= s_{x2C}$	$(\max\{-\sigma_{1T},-\sigma_R\},-\sigma_L]$
$R_E\|R_P$	$s_{xL}\neq s_{x1T}, s_{xR}= s_{x2T}$	$[-\sigma_{1T},\min\{-\sigma_L,-\sigma_R\}]$
$S_P\|S_E$	$s_{xL}= s_{x1C}, s_{xR}\neq s_{x2C}$	$(\max\{-\sigma_L,-\sigma_R\},-\sigma_{2C})$
$S_P\|R_E$	$s_{xL}= s_{x1C}, s_{xR}\neq s_{x2T}$	$(\max\{-\sigma_L,-\sigma_{2T}\},-\sigma_R]$
$R_P\|S_E$	$s_{xL}= s_{x1T}, s_{xR}\neq s_{x2C}$	$(-\sigma_R,\min\{-\sigma_L,-\sigma_{2C}\}]$
$R_P\|R_E$	$s_{xL}= s_{x1T}, s_{xR}\neq s_{x2T}$	$[-\sigma_{2T},\min\{-\sigma_L,-\sigma_R\}]$
$S_E\|S_PS_E$	$s_{xL}\neq s_{x1C}, s_{xR}\neq s_{x2C}$	$(\max\{-\sigma_L,-\sigma_{2C}\},-\sigma_{1C})$
$S_E\|R_PR_E$	$s_{xL}\neq s_{x1C}, s_{xR}\neq s_{x2T}$	$(-\sigma_L,\min\{-\sigma_{1C},-\sigma_{2T}\}]$
$R_E\|S_PS_E$	$s_{xL}\neq s_{x1T}, s_{xR}\neq s_{x2C}$	$(\max\{-\sigma_{1T},-\sigma_{2C}\},-\sigma_L]$
$R_E\|R_PR_E$	$s_{xL}\neq s_{x1T}, s_{xR}\neq s_{x2T}$	$[-\sigma_{1T},\min\{-\sigma_L,-\sigma_{2T}\}]$
$S_P\|S_PS_E$	$s_{xL}= s_{x1C}, s_{xR}\neq s_{x2C}$	$(\max\{-\sigma_L,-\sigma_{2C}\},+\infty)$
$S_P\|R_PR_E$	$s_{xL}= s_{x1C}, s_{xR}\neq s_{x2T}$	$(-\sigma_L,-\sigma_{2T}]$
$R_P\|S_PS_E$	$s_{xL}= s_{x1T}, s_{xR}\neq s_{x2C}$	$(-\sigma_{2C},-\sigma_L]$
$R_P\|R_PR_E$	$s_{xL}= s_{x1T}, s_{xR}\neq s_{x2T}$	$[-Y_0,\min\{-\sigma_L,-\sigma_{2T}\}]$
$S_ES_P\|S_E$	$s_{xL}\neq s_{x1C}, s_{xR}\neq s_{x2C}$	$(\max\{-\sigma_{1C},-\sigma_R\},-\sigma_{2C})$
$S_ES_P\|R_E$	$s_{xL}\neq s_{x1C}, s_{xR}\neq s_{x2T}$	$(\max\{-\sigma_{1C},-\sigma_{2T}\},-\sigma_R]$
$R_ER_P\|S_E$	$s_{xL}\neq s_{x1T}, s_{xR}\neq s_{x2C}$	$(-\sigma_R,\min\{-\sigma_{1T},-\sigma_{2C}\}]$
$R_ER_P\|R_E$	$s_{xL}\neq s_{x1T}, s_{xR}\neq s_{x2T}$	$[-\sigma_{2T},\min\{-\sigma_{1T},-\sigma_R\}]$
$S_ES_P\|S_P$	$s_{xL}\neq s_{x1C}, s_{xR}= s_{x2C}$	$(\max\{-\sigma_{1C},-\sigma_R\},+\infty)$
$S_ES_P\|R_P$	$s_{xL}\neq s_{x1C}, s_{xR}= s_{x2T}$	$(-\sigma_{1C},-\sigma_R]$
$R_ER_P\|S_P$	$s_{xL}\neq s_{x1T}, s_{xR}= s_{x2C}$	$(-\sigma_R,-\sigma_{1T}]$
$R_ER_P\|R_P$	$s_{xL}\neq s_{x1T}, s_{xR}= s_{x2T}$	$[-Y_0,\min\{-\sigma_{1T},-\sigma_R\}]$
$S_ES_P\|S_PS_E$	$s_{xL}\neq s_{x1C}, s_{xR}\neq s_{x2C}$	$(\max\{-\sigma_{1C},-\sigma_{2C}\},+\infty)$
$S_ES_P\|R_PR_E$	$s_{xL}\neq s_{x1C}, s_{xR}\neq s_{x2T}$	$(-\sigma_{1C},-\sigma_{2T}]$
$R_ER_P\|S_PS_E$	$s_{xL}\neq s_{x1T}, s_{xR}\neq s_{x2C}$	$(-\sigma_{2C},-\sigma_{1T}]$
$R_ER_P\|R_PR_E$	$s_{xL}\neq s_{x1T}, s_{xR}\neq s_{x2T}$	$[-Y_0,\min\{-\sigma_{1T},-\sigma_{2T}\}]$

where

$$c_i^n=\begin{cases}\sqrt{\dfrac{4\mu+3K}{3\rho_i^n}}, & \text{if } -\dfrac{2}{3}Y_0<s_{xi}^n<\dfrac{2}{3}Y_0,\\[2ex] \sqrt{(a_i^n)^2-\dfrac{(\gamma-1)s_{xi}^n}{\rho_i^n}}, & \text{if } s_{xi}^n=\dfrac{2}{3}Y_0 \text{ or } s_{xi}^n=-\dfrac{2}{3}Y_0.\end{cases}\tag{5.2}$$

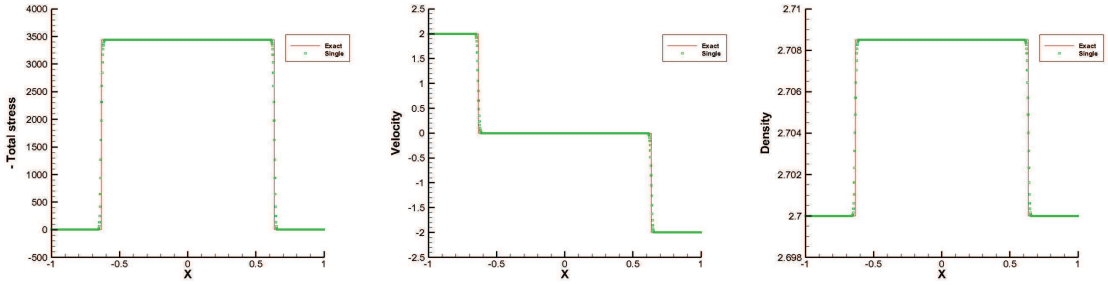
https://doi.org/10.4208/aamm.2015.m1340 Published online by Cambridge University Press

5.1 Numerical justifications of the exact elastic solid-solid Riemann solver

Test 5.1. The numerical justification of the exact elastic solid-solid Riemann solver with solution type $S_E|S_E$. Unless explicitly stated, the solid material is assumed to be the aluminium with nondimensional physical parameters $\rho_0=2.71$, $c_0=538.0$, $\gamma=2.67$, $K=740000.0$, $\mu=265000.0$, $Y_0=3000.0$. The nondimensional initial conditions are

$$\begin{cases} u_L=2.0, & p_L=1.0, & \rho_L=2.7, & s_L=0.0, \\ u_R=-2.0, & p_R=1.0, & \rho_R=2.7, & s_R=0.0. \end{cases} \tag{5.3}$$

The computational domain is set to be $[-1,1]$ with 2000 uniform grid points and initial interface is located at 0.0. Besides, the CFL number is 0.9 and the terminal time is 0.001. As shown in Fig. 5, the exact solution matches the numerical results well.



(a) − Total stress (b) Velocity (c) Density

Figure 5: The numerical justification of the exact elastic solid-solid Riemann solver with solution type $S_E|S_E$.

Test 5.2. The numerical justification of the exact elastic solid-solid Riemann solver with solution type $R_E|R_E$. The nondimensional initial conditions are

$$\begin{cases} u_L=-2.0, & p_L=3000.0, & \rho_L=2.7, & s_L=0.0, \\ u_R=2.0, & p_R=3000.0, & \rho_R=2.7, & s_R=0.0. \end{cases} \tag{5.4}$$

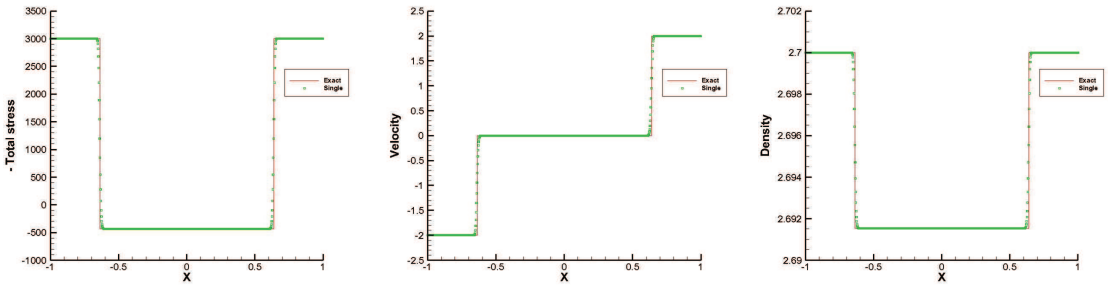
The computational domain is set to be $[-1,1]$ with 2000 uniform grid points and initial interface is located at 0.0. The CFL number is 0.9 and the terminal time is 0.001. As shown in Fig. 6, the exact solution also matches the numerical results well.

5.2 Numerical justifications of the exact perfectly plastic solid-solid Riemann solver

Test 5.3. The numerical justification of the exact perfectly plastic solid-solid Riemann solver with solution type $S_P|S_P$. The nondimensional initial conditions are

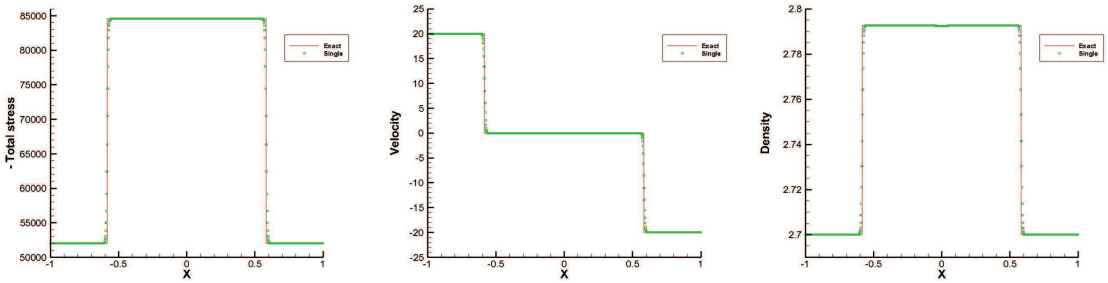
$$\begin{cases} u_L=20.0, & p_L=50000.0, & \rho_L=2.7, & s_L=-2000.0, \\ u_R=-20.0, & p_R=50000.0, & \rho_R=2.7, & s_R=-2000.0. \end{cases} \tag{5.5}$$

https://doi.org/10.4208/aamm.2015.m1340 Published online by Cambridge University Press



(a) − Total stress (b) Velocity (c) Density

Figure 6: The numerical justification of the exact elastic solid-solid Riemann solver with solution type $R_E|R_E$.



(a) − Total stress (b) Velocity (c) Density

Figure 7: The numerical justification of the exact perfectly plastic solid-solid Riemann solver with solution type $S_P|S_P$.

The computational domain is set to be $[-1,1]$ with 2000 uniform grid points and initial interface is located at 0.0. The CFL number is 0.9 and the terminal time is 0.001. As shown in Fig. 7, the exact solution matches the numerical results well.

Test 5.4. The numerical justification of the exact perfectly plastic solid-solid Riemann solver with solution type $R_P|R_P$. The nondimensional initial conditions are

$$\begin{cases} u_L=-20.0, & p_L=50000.0, & \rho_L=2.7, & s_L=2000.0, \\ u_R=20.0, & p_R=50000.0, & \rho_R=2.7, & s_R=2000.0. \end{cases} \tag{5.6}$$

The computational domain is set to be $[-1,1]$ with 2000 uniform grid points and initial interface is located at 0.0. The CFL number is 0.9 and the terminal time is 0.001. As shown in Fig. 8, the exact solution also matches the numerical results well.

https://doi.org/10.4208/aamm.2015.m1340 Published online by Cambridge University Press

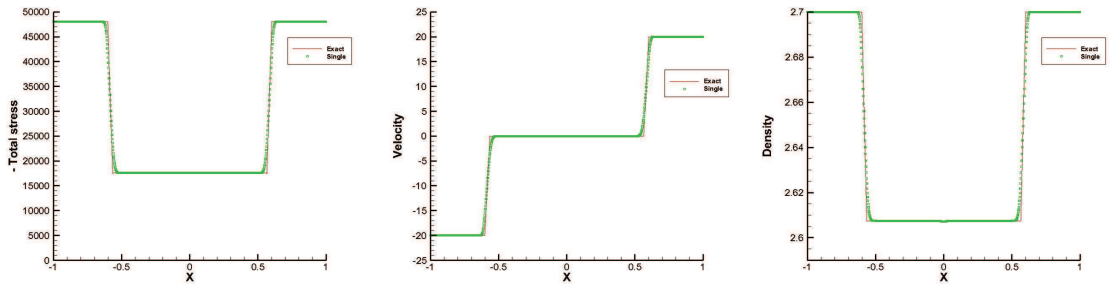
5.3 Numerical justifications of the exact elastic-perfectly plastic solid-solid Riemann solver

Test 5.5. The numerical justification of the exact elastic-perfectly plastic solid-solid Riemann solver with solution type $S_E S_P | S_P S_E$. The nondimensional initial conditions are

$$\begin{cases} u_L = 20.0, & p_L = 1.0, & \rho_L = 2.7, & s_L = 0.0, \\ u_R = -20.0, & p_R = 1.0, & \rho_R = 2.7, & s_R = 0.0. \end{cases} \tag{5.7}$$

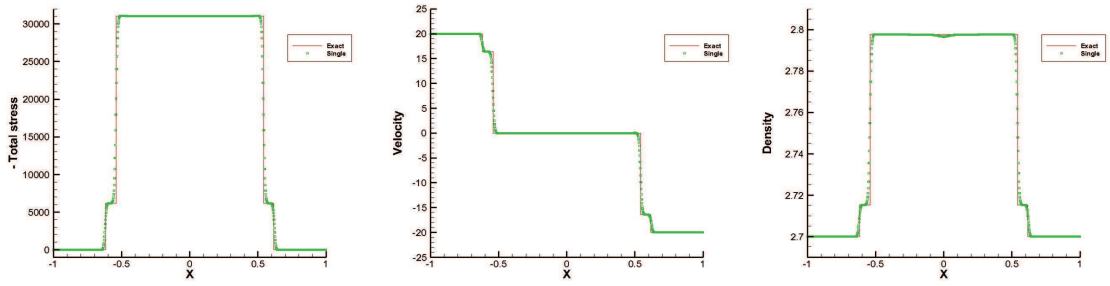
The computational domain is set to be $[-1,1]$ with 2000 uniform grid points and initial interface is located at 0.0. Besides, the CFL number is 0.9 and the terminal time is 0.001. As shown in Fig. 9, the exact solution matches the numerical results well generally, but notice that there is a slight undershooting of the Lax-Friedrichs scheme in the density figure because of the effect of overheating [27].

Test 5.6. The numerical justification of the exact elastic-perfectly plastic solid-solid Rie-



(a) − Total stress (b) Velocity (c) Density

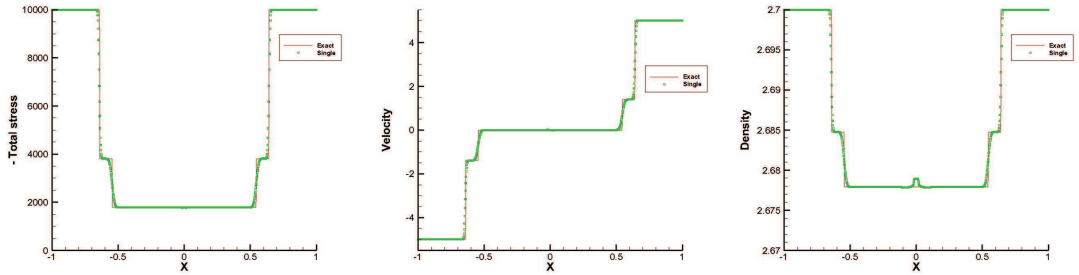
Figure 8: The numerical justification of the exact perfectly plastic solid-solid Riemann solver with solution type $R_P | R_P$.



(a) − Total stress (b) Velocity (c) Density

Figure 9: The numerical justification of the exact elastic-perfectly plastic solid-solid Riemann solver with solution type $S_E S_P | S_P S_E$.

https://doi.org/10.4208/aamm.2015.m1340 Published online by Cambridge University Press



(a) − Total stress (b) Velocity (c) Density

Figure 10: The numerical justification of the exact elastic-perfectly plastic solid-solid Riemann solver with solution type $R_ER_P|R_PR_E$.

mann solver with solution type $R_ER_P|R_PR_E$. The nondimensional initial conditions are

$$\begin{cases} u_L=-5.0, & p_L=10000.0, & \rho_L=2.7, & s_L=0.0, \\ u_R=5.0, & p_R=10000.0, & \rho_R=2.7, & s_R=0.0. \end{cases} \tag{5.8}$$

The computational domain is set to be $[-1,1]$ with 2000 uniform grid points and initial interface is located at 0.0. Besides, the CFL number is 0.9 and the terminal time is 0.001. As shown in Fig. 10, the exact solution matches the numerical results well generally, but there is a slight overshooting of the Lax-Friedrichs scheme in the density figure because of the effect of overheating as well.

5.4 Convergence verification of the exact elastic-perfectly plastic solid-solid Riemann solver

When the grid points are refined, if the proposed elastic-perfectly plastic solid-solid Riemann solver is exact, the result computed by the Lax-Friedrichs scheme will converge to the outcome calculated by this Riemann solver. For example, if we refine the uniform grid points from 2000 to 4000 and 8000 within the computational domain $[-1,1]$ of Test 5.5, the L_1-errors of total stress, velocity and density will converge to 0 respectively, as shown in Table 2. In addition, owing to the existence of shock waves, the spatial accuracy of the Lax-Friedrichs scheme is less than 1-order.

Table 2: Convergence verification of Test 5.5 with solution type $S_ES_P|S_PS_E$.

	Total stress		Velocity		Density	
Δx	L_1-error	Order	L_1-error	Order	L_1-error	Order
0.001	484.885		0.311894		0.001639	
0.0005	294.643	0.718676	0.189059	0.722219	0.000986	0.733156
0.00025	171.633	0.779644	0.109635	0.786128	0.000566	0.800786

https://doi.org/10.4208/aamm.2015.m1340 Published online by Cambridge University Press

6 Multi-material extension

Since the exact elastic-perfectly plastic solid Riemann solver has been verified, we apply this Riemann solver to the multi-material problem, specifically the fluid-solid interaction. To decouple the fluid-solid interface, we employ the modified ghost fluid method (MGFM) raised by Liu et al. [10] who modified the original ghost fluid method (GFM) [29]. MGFM is a more accurate and effective approach, which defines the ghost fluid status by solving a local multi-material Riemann problem at the interface instead of the pressure and velocity assignment and entropy extrapolation used in the original GFM. Hence, the exact elastic-perfectly plastic solid Riemann solver discussed in section 4 can be extended to the multi-material case and then included in the MGFM approach to decouple the multi-material interaction. Besides, although the Riemann solver is one-dimensional, GFM-based methods can easily extend to the multi-dimensional cases via using the one-dimensional solver along the normal direction of the multi-material interfaces. And much work [10–12, 29] has manifested that the GFM-based methods own the ability to combine the advantages of front capturing and front tracking approaches.

6.1 Governing equations and equations of state for the fluid

For the one dimensional compressible fluid, governing equations are Euler equations in the conservative form, neglecting the effects of body force, viscous stresses and heat-conducting, given by

$$\frac{\partial U}{\partial t}+\frac{\partial F(U)}{\partial x}=0, \tag{6.1}$$

where

$$U=\begin{pmatrix}\rho\\ \rho u\\ E\end{pmatrix},\quad F(U)=\begin{pmatrix}\rho u\\ \rho u^2+p\\ (E+p)u\end{pmatrix}.$$

For closure of system (6.1), equation of state is required. The $\gamma-$law for the compressible gas is

$$p(\rho,e)=(\gamma_g-1)\rho e, \tag{6.2}$$

where γ_g is the specific heat ratio for the particular gas and is set equal to 1.4 for the air. The equation of state for the compressible water is the Tait equation of state

$$p(\rho,e)=(\gamma_w-1)\rho e-\gamma_w(B-A), \tag{6.3}$$

where A, B and the specific heat ratio for water γ_w are constants, $A=10^5$Pa, $B=3.31\times 10^8$Pa, $\gamma_w=7.15$.

6.2 The exact fluid elastic-perfectly plastic solid Riemann solver

Suppose that the fluid and the elastic-perfectly plastic solid are located at the left and right sides of the interface respectively, the one-dimensional fluid elastic-perfectly plastic

https://doi.org/10.4208/aamm.2015.m1340 Published online by Cambridge University Press

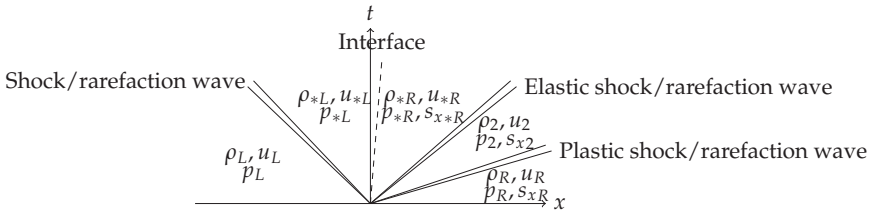


Figure 11: Four-wave solution structure of the fluid elastic-perfectly plastic solid Riemann problem.

solid Riemann problem in the vicinity of the interface can be described in the Euler-Euler coordinate system as

$$\begin{cases} \dfrac{\partial U}{\partial t}+\dfrac{\partial F(U)}{\partial x}=0 \quad \text{with } U|_{t=0}=U_L \text{ for } x<x_0, \\ \dfrac{\partial V}{\partial t}+\dfrac{\partial G(V)}{\partial x}=0 \quad \text{with } V|_{t=0}=V_R \text{ for } x>x_0, \end{cases} \tag{6.4}$$

where the left constant state U_L and right constant state V_R are separated by the the interface located at x_0. For the one-dimensional gas-gas or gas-water multi-material Riemann problem, study finds that the solution structure is similar to the pure gas Riemann problem, neglecting vacuum or cavitation effects in fluid [28]. And the contact discontinuity is exactly the multi-material interface. Therefore, it is reasonable to assume that the fluid elastic-perfectly plastic solid Riemann solution consists of five constant states $(U_L,U_{*L},V_{*R},V_2,V_R)$ connected by four elementary waves when the solid undergoes the elastic-plastic phase transition, see Fig. 11. Otherwise, if the solid has not underwent the elastic-plastic phase transition, the solution consists of four constant states (U_L,U_{*L},V_{*R},V_R) connected by three elementary waves. To propose the Riemann solver for the fluid elastic-perfectly plastic solid Riemann problem (6.5), the core strategy is iterating the pressure p_{*L} in fluid and the negative total stress $-\sigma_{*R}$ in solid.

Proposition 6.1. For the four-wave solution structure, the solution of pressure p_{*L} in fluid and negative total stress $-\sigma_{*R}$ in solid for the multi-material Riemann problem (6.5) is given by the root of the algebratic equation

$$h(p_*,W_L,W_R):=f_L|(p_*,W_L)+g_R|_{PE}(p_*,W_R)+u_R-u_L=0, \tag{6.5}$$

with

$$p_*=p_{*L}=-\sigma_{*R},$$

https://doi.org/10.4208/aamm.2015.m1340 Published online by Cambridge University Press

Table 3: Auxiliary condition and solution interval of each type for the complete exact fluid elastic-perfectly plastic solid Riemann solver.

Solution type	Auxiliary condition	Solution interval
$S\|S_E$	$s_{xR}\neq s_{x2C}$	$[\max\{p_L,-\sigma_R\},-\sigma_{2C}]$
$S\|R_E$	$s_{xR}\neq s_{x2T}$	$[\max\{p_L,-\sigma_{2T}\},-\sigma_R]$
$R\|S_E$	$s_{xR}\neq s_{x2C}$	$[-\sigma_R,\min\{p_L,-\sigma_{2C}\}]$
$R\|R_E$	$s_{xR}\neq s_{x2T}$	$[-\sigma_{2T},\min\{p_L,-\sigma_R\}]$
$S\|S_P$	$s_{xR}=s_{x2C}$	$[\max\{p_L,-\sigma_R\},+\infty]$
$S\|R_P$	$s_{xR}=s_{x2T}$	$[p_L,-\sigma_R]$
$R\|S_P$	$s_{xR}=s_{x2C}$	$[-\sigma_R,p_L]$
$R\|R_P$	$s_{xR}=s_{x2T}$	$[0,\min\{p_L,-\sigma_R\}]$
$S\|S_PS_E$	$s_{xR}\neq s_{x2C}$	$[\max\{p_L,-\sigma_{2C}\},+\infty]$
$S\|R_PR_E$	$s_{xR}\neq s_{x2T}$	$[p_L,-\sigma_{2T}]$
$R\|S_PS_E$	$s_{xR}\neq s_{x2C}$	$[-\sigma_{2C},p_L]$
$R\|R_PR_E$	$s_{xR}\neq s_{x2T}$	$[0,\min\{p_L,-\sigma_{2T}\}]$

where $f_L(p_*,W_L)$ is given by one of the following four expressions

$$f_L^S|_g(p_*,W_L)=\sqrt{(p_*-p_L)\left[\frac{1}{\rho_L}-\frac{1}{\rho_{*L|g}}\right]}, \qquad \text{if } p_*>p_L, \tag{6.6a}$$

$$f_L^S|_w(p_*,W_L)=\sqrt{(p_*-p_L)\left[\frac{1}{\rho_L}-\frac{1}{\rho_{*L|w}}\right]}, \qquad \text{if } p_*>p_L, \tag{6.6b}$$

$$f_L^R|_g(p_*,W_L)=\frac{2a_{L|g}}{\gamma_g-1}\left[\left(\frac{p_*}{p_L}\right)^{\frac{\gamma_g-1}{2\gamma_g}}-1\right], \qquad \text{if } p_*\leq p_L, \tag{6.6c}$$

$$f_L^R|_w(p_*,W_L)=\frac{2a_{L|w}}{\gamma_w-1}\left[\left(\frac{p_*+B-A}{p_L+B-A}\right)^{\frac{\gamma_w-1}{2\gamma_w}}-1\right], \qquad \text{if } p_*\leq p_L, \tag{6.6d}$$

with

$$\frac{\rho_{*L|g}}{\rho_L}=\frac{(\gamma_g+1)p_*+(\gamma_g-1)p_L}{(\gamma_g+1)p_L+(\gamma_g-1)p_*}, \qquad \frac{\rho_{*L|w}}{\rho_L}=\frac{(\gamma_w+1)p_*+(\gamma_w-1)p_L+2\gamma_w(B-A)}{(\gamma_w+1)p_L+(\gamma_w-1)p_*+2\gamma_w(B-A)},$$

$$a_{L|g}=\sqrt{\frac{\gamma_g p_L}{\rho_L}}, \qquad a_{L|w}=\sqrt{\frac{\gamma_w(p_L+B-A)}{\rho_L}},$$

and $g_R|_{PE}(p_*,W_R)$ is given by Eq. (4.9a) or (4.10). Subscripts "g" and "w" at the right side of the vertical bar represent the expression is utilized for the material of "gas" and "water".

Similarly, for the three-wave solution structure, its exact Riemann solver can be obtained by referring to the Proposition 6.1. In this case, solution types include $S|S_E$, $S|R_E$,

https://doi.org/10.4208/aamm.2015.m1340 Published online by Cambridge University Press

$R|S_E$, $R|R_E$, $S|S_P$, $S|R_P$, $R|S_P$, $R|R_P$. For the four-wave solution structure, solution types include $S|S_PS_E$, $S|R_PR_E$, $R|S_PS_E$, $R|R_PR_E$. Again, given that the initial states have been provided, to decide which solution type is true, it can be searched one by one as listed in the Table 3, judging by its auxiliary condition and solution interval which the exact solution has to be in. These twelve solution types construct the complete exact fluid elastic-perfectly plastic solid Riemann solver.

7 Multi-material applications

Test 7.1. Water-aluminium Riemann problem with solution type $S|S_PS_E$. The nondimensional initial conditions are

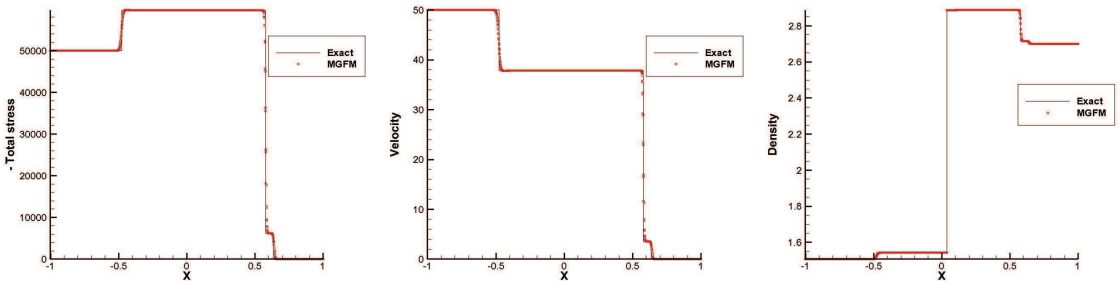
$$\begin{cases} u_L=50.0, & p_L=50000.0, & \rho_L=1.507, \\ u_R=0.0, & p_R=1.0, & \rho_R=2.7, \quad s_R=0.0. \end{cases} \tag{7.1}$$

The computational domain is set to be $[-1,1]$ with 2000 uniform grid points and initial interface is located at 0.0. Besides, the CFL number is 0.9 and the terminal time is 0.001. As shown in Fig. 12, the exact solution matches the MGFM results well.

Test 7.2. Gas-aluminium Riemann problem with solution type $R|S_PS_E$. The nondimensional initial conditions are

$$\begin{cases} u_L=50.0, & p_L=100000.0, & \rho_L=3.0, \\ u_R=0.0, & p_R=1.0, & \rho_R=2.7, \quad s_R=0.0. \end{cases} \tag{7.2}$$

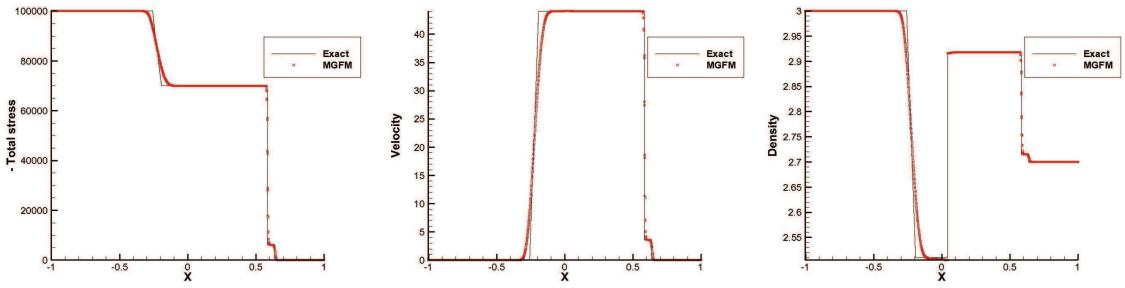
The computational domain is set to be $[-1,1]$ with 2000 uniform grid points and initial interface is located at 0.0. Besides, the CFL number is 0.9 and the terminal time is 0.001. As shown in Fig. 13, the exact solution matches the MGFM results well.



(a) − Total stress (b) Velocity (c) Density

Figure 12: The result comparison of the exact water elastic-perfectly plastic solid Riemann solver versus the MGFM with solution type $S|S_PS_E$.

https://doi.org/10.4208/aamm.2015.m1340 Published online by Cambridge University Press



(a) − Total stress (b) Velocity (c) Density

Figure 13: The result comparison of the exact gas elastic-perfectly plastic solid Riemann solver versus the MGFM with solution type $R|S_PS_E$.

8 Conclusions

In this work, we propose an exact elastic-perfectly plastic solid Riemann solver and extend it to the multi-material case which can be utilized to decouple the fluid elastic-perfectly plastic solid interaction. The analysis of the elastic-perfectly plastic solid Riemann problem is based on dismantling the complicated non-linear wave relations into two segments, the elastic wave relation and the plastic wave relation, and then combining them together via employing the mechanism of the elastic-plastic phase transition. Numerical examinations of this exact Riemann solver and its multi-material applications also demonstrate that the method is feasible and effective.

References

[1] S. K. GODUNOV, *A finite difference method for the computation of discontinuous solutions of the equations of fluid dynamics,* Mat. Sb., 47 (1959), pp. 357–393.
[2] E. F. TORO, Riemann Solvers and Numerical Methods for Fluid Dynamics: A Practical Introduction, 3th ed., Springer-Verlag, 2009.
[3] B. EINFELDT, *On Godunov-Type methods for gas dynamics,* SIAM J. Numer. Anal., 25 (1988), pp. 294–318.
[4] B. EINFELDT, C. D. MUNZ, P. L. ROE AND B. SJÖGREEN, *On Godunov-Type methods near low densities,* J. Comput. Phys., 92 (1991), pp. 273–295.
[5] A. HATEN, P. D. LAX AND B. VAN LEER, *On upstream differencing and Godunov-type schemes for hyperbolic conservation laws,* SIAM Rev., 25 (2002), pp. 35–61.
[6] E. F. TORO, M. SPURSE AND W. SPEARES, *Restoration of the contact surface in the HLL-Riemann solver,* Shock Waves, 4 (1994), pp. 25–34.
[7] P. L. ROE, *Approximate Riemann solvers, parameter vectors, and difference schemes,* J. Comput. Phys., 43 (1981), pp. 357–372.
[8] B. ENGQUIST AND S. OSHER, *One sided difference approximations for nonlinear conservation laws,* Math. Comput., 36 (1981), pp. 321–351.

https://doi.org/10.4208/aamm.2015.m1340 Published online by Cambridge University Press

[9] S. Osher and F. Solomon, *Upwind difference schemes for hyperbolic conservation laws,* Math. Comput., 38 (1982), pp. 339–374.
[10] T. G. Liu, B. C. Khoo and K. S. Yeo, *Ghost fluid method for strong shock impacting on material interface,* J. Comput. Phys., 190 (2003), pp. 651–681.
[11] T. G. Liu, W. F. Xie and B. C. Khoo, *The modified ghost fluid method for coupling of fluid and structure constituted with Hydro-Elasto-Plastic equation of state,* SIAM J. Sci. Comput., 33 (2008), pp. 1105–1130.
[12] T. G. Liu, A. W. Chowdhury and B. C. Khoo, *The modified ghost fluid method applied to fluid-elastic structure interaction,* Adv. Appl. Math. Mech., 3 (2011), pp. 611–632.
[13] A. Kaboudian and B. C. Khoo, *The ghost solid method for the elastic solid-solid interface,* J. Comput. Phys., 257 (2014), pp. 102–125.
[14] P. G. LeFloch and F. Olsson, *A second-order Godunov method for the conservation laws of nonlinear elastidynamics,* Impact Comput. Sci. Eng., 2 (1990), pp. 318–354.
[15] X. Garaizar, *Solution of a Riemann problem for elasticity*, J. Elasticity., 26 (1991), pp. 43–63.
[16] G. H. Miller, *An iterative Riemann solver for systems of hyperbolic conservation laws, with application to hyperelastic solid mechanics,* J. Comput. Phys., 193 (2003), pp. 198–225.
[17] P. T. Barton, D. Drikakis, E. Romenski and V. A. Titarev, *Exact and approximate solutions of Riemann problems in non-linear elasticity,* J. Comput. Phys., 228 (2009), pp. 7046–7068.
[18] A. López Ortega, M. Lombardini, D. I. Pullin and D. I. Meiron, *Numerical simulation of elastic-plastic solid mechanics using an Eulerian stretch tensor approach and HLLD Riemann solver,* J. Comput. Phys., 257 (2014), pp. 414–441.
[19] J. A. Trangenstein and R. B. Pember, *The Riemann problem for longitudinal motion in an elastic-plastic bar,* SIAM J. Sci. State. Comput., 12 (1991), pp. 180–207.
[20] X. Lin, Numerical Computation of Stress Waves in Solids, Akademie Verlag, 1996.
[21] F. Wang, J. G. Glimm, J. W. Grove, B. J. Plohr and D. H. Sharp, *A conservative Eulerian numerical scheme for elasto-plasticity and application to plate impact problems,* Impact Comput. Sci. Eng., 5 (1993), pp. 285–308.
[22] B. Plohr and B. Sharp, *A conservative formulation for plasticity,* Adv. Appl. Math., 13 (1992), pp. 462–493.
[23] G. H. Miller and P. Colella, *A high-order Eulerian Godunov Method for elastic-plastic flow in solids*, J. Comput. Phys., 167 (2001), pp. 131–176.
[24] J. A. Trangenstein and P. Colella, *A higher-order Godunov method for modeling finite deformation in elastic-plastics solids,* Commun. Pure Appl. Math., 44 (1991), pp. 41–100.
[25] M. L. Wilkins, *Calculation of elastic-plastic flow,* Meth. Comput. Phys., 3 (1964), pp. 211–263.
[26] H. S. Tang and F. Sotiropoulos, *A second-order Godunov method for wave problems in coupled solid-water-gas systems,* J. Comput. Phys., 151 (1999), pp. 790–815.
[27] R. P. Fedkiw, A. Marquina and B. Merriman, *An isobaric fix for the overheating problem in multimaterial compressible flows,* J. Comput. Phys., 148 (1999), pp. 545–578.
[28] J. Smooler, Shock Waves and Reaction-Diffusion Equations, Springer-Verlag, 1983.
[29] R. P. Fedkiw, T. Aslam, B. Merriman and S. Osher, *A non-oscillatory Eulerian approach to interfaces in multimaterial flows (the Ghost Fluid Method),* J. Comput. Phys., 152 (1999), pp. 457–492.
[30] Y. H. Guo, R. Li and C. B. Yao, *A numerical method on Eulerian grids for two-phase compressible flow,* Adv. Appl. Math. Mech., 8 (2016), pp. 187–212.
[31] L. Xu and T. G. Liu, *Modified ghost fluid method as applied to fluid-plate interaction,* Adv. Appl. Math. Mech., 6 (2014), pp. 24–48.

https://doi.org/10.4208/aamm.2015.m1340 Published online by Cambridge University Press